International Journal of Current Advanced Research
ISSN: O: 2319-6475, ISSN: P: 2319-6505, Impact Factor: 6.614
Available Online at www.journalijcar.org
Volume 11; Issue 04 (C); April 2022; Page No.697-703
DOI: http://dx.doi.org/10.24327/ijcar.2022.703.0158

Research Article

A COMPARATIVE ANALYSIS INVOLVING DNCNN AND PCA ON Φ-OTDR VIBRATION SENSING

Atubga David Atia Ibrahim[1], Khushnood Abbas[2], and Bonny Ernestina Linda[3]

[1]The National Key Lab of Optical Fiber Sensing Systems of Ministry of Education, China School of Information and Communication Engineering, University of Electronic Science and Technology of China
[2]School of Computer Science and Technology, Zhoukou Normal University
[3]School of Management Science and Economics, University of Electronic Science and Technology of China

A R T I C L E I N F O

Article History:
Received 15th January, 2022
Received in revised form 7th February, 2022
Accepted 13th March, 2022
Published online 28th April, 2022

Key words:
Denoising Convolutional Neural Network (DnCNN), Phase-sensitive Optical Time Domain Reflectometry (Φ-OTDR), Principal Component Analysis (PCA), Signal-to-Noise-Ratio (SNR)

A B S T R A C T

In Distributed Optical Fiber Sensors (DOFS), the Phase-sensitive Optical Time Domain Reflectometry (Φ-OTDR) technology has tremendously demonstrated stupefying performance with regard to measurements of real-time accurate positioning of trains, intrusion detection, all due to its unique prospects on high sensitivity and precision, fast speed response, long distance sensing, everlasting lifetime service, and above all, low operational cost. Nonetheless, its application for vibration detection becomes stressful should the data is impeded by harsh external conditions. Hence to successfully enhance its smooth application, we investigated and executed a robust deep learning algorithm-Denoising Convolutional Neural Network (DnCNN) on Φ-OTDR sensing data for vibration detection. We utilized 60 exquisite layers comprising ReLU, 2Dconvolutional, batch normalization in order to improve the training speed and denoising performanceand finally a regression layer. The trained network (TrainedNet), was successfully performed after obtaining Digital Down Conversion (DDC) of the Φ-OTDR noisy data. The target of locating the vibration point was smoothly harnessed at a distance of approximately 50m and the proposed DnCNN technique was then evaluated against one state-of-the-art denoising algorithm and it outperformed it. The theoretical analysis and simulated demonstrations of the preceding locations under the sensing distance of 200m are hereby presented as proof of concept.

INTRODUCTION

In recent times, Distributed optical fiber sensing (DOFS) systems have been broadly used in varied industries with regard to health structural monitoring and security surveillance due to their immunity to large-scale monitoring, simple installation, geometric versatility as well as low cost per monitored point [1]. There have been a cross-sectional analysis of these with respect to sensing parameters [2], monitoring range [3], spatial resolution [4], vibration detection [5], among others. As one of the typical DOFS systems, the Phase-sensitive Optical Time Domain Reflectometry (Φ-OTDR) is one of the most vigorous and integral part of the distributed optical fiber sensing technologies, the Φ-OTDR is known to be an effective tool for border intrusion monitoring with respect to detecting and locating one or more vibration events occurring along the sensing fiber [6] [7]. The application of the said sensing technology becomes stressful should the data meant for vibration detection is impeded my noise. Hence, The CNNs has greatly demonstrated its strength in enhancing the sensing performance of 2Draw data of Raman OTDR [8], event recognition and classification, as well as strain prediction of Rayleigh backscatter spectra with noise tolerance and improved resolution [9–16]. In [17], the CNN was successfully applied on specific experimental datasets involving wavelet scanning coherent optical time domain frequency dimensions. Deep learning in recent times has greatly demonstrated significant impact in signal processing. The denoising DnCNN [18-19] consisting of convolutions, batch normalization (BN) [20], rectified linear unit (ReLU) [21] and residual learning (RL) [22], [23] was successfully applied for JPEG image deblocking, image denoising, and for super-resolution enhancement. In the BOTDA sensing system, the DnCNN model was also applied of which improved SNR values of 13.43 dB, 13.57 dB, and 12.9 dB are achieved at 500 MSa/s, 250 MSa/s, and 125 MSa/s sampling rate, accordingly [24] [25]. Hence, the DnCNN approach was successfully investigated and applied for denoising the Φ-OTDR signal after performing an effective training of the model. The quest to detecting the vibration point was smoothly executed with a significant enhancement of the SNR value from 15dB to 36.6dB. The efficacy of the proposed model was evaluated against another state-of-the-art denoising technique. The next section introduces the theoretical basis of the Φ-OTDR sensing

Corresponding author:* **Atubga David Atia Ibrahim
The National Key Lab of Optical Fiber Sensing Systems of Ministry of Education, China School of Information and Communication Engineering, University of Electronic Science and Technology of China

system whereas Section 3 presents the proposed method while Section 4 illustrates the results and discussions, and Section 5 concludes the paper.

Theoretical Basis of the Φ-OTDR Sensing System

Basic Principle of Φ-OTDR Technology

Figure 1 gives an illustration of the Φ-OTDR system. The said sensing technology which is the OTDR prototype was initially demonstrated by Henry F. Taylor in 1993 [26]. It has since noted as one of the key distributed optical fiber sensing technologies. Traditionally, the working principle of the two systems is related, and compared to the broadband light source used by the conventional OTDR system, the Φ-OTDR system uses ultranarrow line width lasers as its main source of light. It receives and uses the interference effect between the backward Rayleigh light in the wide pulse, then injects the high coherent light into the sensing fiber and the reflected coherent Rayleigh scattered light is detected by the detector [27]. The Φ-OTDR system has the advantage of high sensitivity as well as a longer distance sensing ability. Apparently, the Φ-OTDR can principally enhance direct detection and coherent detection of two structures. These attributes are the main difference between the two systems [27].

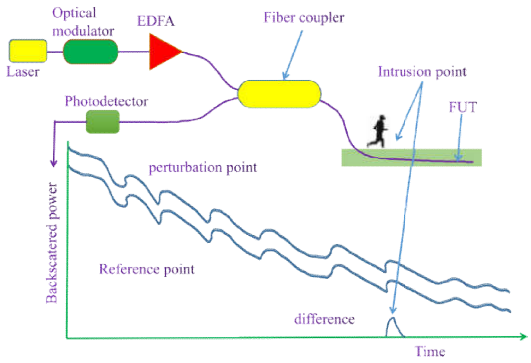

Fig 1 The working Principle of the Φ-OTDR system

Significantly, the advantage of direct detection by the Φ-OTDR system is known to be relatively low in terms of cost. Also, its data processing method and structure are quite simple. The main disadvantage of coherent detection for the Φ-OTDR system is the strict requirement on the coherence of light source [27].In the orientation of the Φ-OTDR system when there is perturbation on the fiber at a certain point, the internal refractive index and the length of the fiber at that location will change, thereby resulting in a change in the optical phase of the optical interference [27]. This change therefore leads to backward Rayleigh scattering light intensity, which means that the backward optical power changes and will be disturbed when the scattering power curve subtracts the power curve without disturbance. Hence, the distance of the disturbed signal, according to the light in the fiber speed as well as the signal transmission time of the corresponding relationship and disturbance information, can be positioned accurately [28].

Methodological Approach

Frequency Shift for A Zero-Band Signal Acquisition

In order to effectively facilitate smooth training of the DnCNN model towards the desired denoising output, we first performed digital down-conversion frequency shift on the Φ-OTDR simulated mid-band signal to enhance a zero-band signal by applying Hilbert Transform as presented beneath in Eq. (1).

$$\rho(t) = hbt[I(t)] \tag{1}$$

of which $hbt[I(t)]$ is indicated as Hilbert transform so that $\rho(t)$ could be retrieved successfully. Therefore, the mid-frequency band signal was effectively enhanced by the application of Eq. (2) as illustrated below

$$\mathcal{E}^{beat} = I(t) + j\rho(t) \tag{2}$$

whereby $\mathcal{E}^{beat}$ represents the mid-frequency band signal, while $\rho(t)$ represents the imaginary signal and $I(t)$ denotes the real signal. Finally, the digital frequency down-conversion execution was successfully performed to achieve the zero-band signal using Eq. (3) below

$$\mathcal{E} = \mathcal{E}^{beat} \cdot exp(-j2\pi ft) \tag{3}$$

Where $\mathcal{E}$ represents the zero-band signal. Hence, the application of the DnCNN model for training towards the achievement of the desired denoising outcome was performed after obtaining the Digital Down Conversion DDC noisy data. The illustration of the DDC approach is therein presented below in Fig. 2.

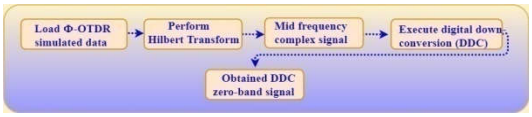

Fig 2 Frequency shift for Zero-band signal

DnCNN Architecture

The DnCNN architecture is comprised of three principal operators such as: Convolution (Conv), Batch Normalization (BN), and the Rectified Linear Units (ReLU). The main function of the convolution operator is to enhance the extraction of different feature maps from images using different convolutional filters. As a result in shallow layers, the elementary visual features such as edges, end-points, corners are obtained and further combined with higher layers to learn the characteristics of the inputs in order to enhance effective filtering. Emphatically stating, the preceding capabilities give the approach a distinctive feature of been able to recognize or restore the required results. Nevertheless, it is always challenging to train the net solely with convolution operator hence, the BN and ReLU are incorporated to facilitate the training process as presented in Fig. 3 below.

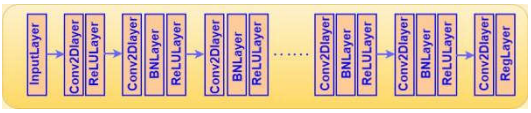

Fig 3 DnCNN Architecture

The BN operator is integrated to extensively speed up the training process and also boost the denoising performance [20]. It is capable of solving the internal co-variate shift (ICS) related problems that occur during the training process. The said problems emanate as a result of the changes in the distribution of the input from each layer during the training processes due to the changes in the parameters of the previous layers. The ICS poses treats on the training model thereby slowing down the process. Hence, normalizing the input of each layer is always handled smoothly by the BN operation to greatly reduces the ICS related constraints. In addition, the activation function on the other hand is equally incorporated to add nonlinear factors in

order to solve more complex difficulties. As one of the most prominent activation functions, using the ReLU facilitates the network to converge faster during the training processes and the gradient vanishing problem will be effectively controlled. As a result, by successfully combining the convolution operation with ReLU [19], the DnCNN can gradually and effectively separate the desired image constituents from the noisy observation through the hidden layers. The data presented exhibits the dimensions of 4000×4000 of which the depth of DnCNN is chosen to be 20, whereby the patches size of the receptive field is $50 \times 50 \times 2$. The 20 layers can be divided into three types: (1) the first layer is comprised of 64 filters with a size of 3×3 used to construct 64 feature mapping the noisy input data, of which the ReLU is then utilized for nonlinearity; (2) From layers 2-19, 64 filters of size $64 \times 3 \times 3$ are used, whereby the BN is added in-between the convolution and ReLU functions; (3) Then a $3 \times 3 \times 2$ size filter is used to reconstruct the final outputs.

$$l(\Theta) = \frac{1}{2N}\sum_{i=1}^{N} \left\| R(x_i;\Theta) - (x_i - y_i) \right\|_F^2 \qquad (4)$$

The input for the DnCNN training process is represented as anoisy observation of $u = x + y$, where y is the clean data and u is indicated as the noise. Therefore, in the DnCNN training process, the noise learning formulation is adopted to train a noise mapping $R(u) \approx x$, and then the clean signal can be obtained by $x = y - R(y)$ [21]. The noise output is then normalized using batch normalization. Eq. (4) is the loss function of the DnCNN approach, which is the average mean squared error between the noise and estimated ones from the nosy input [22]. Therefore to minimize the value of (4), the DnCNN is trained to obtain the features of noise u from the noise data x. Behind the propagation phase of the training process, the Θ which is the trainable parameters of each Conv, BN and ReLU are automatically adjusted to minimize the loss function. In the training, the DnCNN can effectively estimate the distribution of noise from the noisy input data based on the acquired knowledge. The next section presents the discussion of the DnCNN training process.

Denoising constraints and training technique

In this study, instead of expressly learning and following the pattern of a discriminatory modeling approach, we explored and handled the Φ-OTDR signal denoising process as an obvious selective learning problem using the DnCNN scheme. The performance of the general 2D image denoising techniques using ANNs involving the CNNs have demonstrated tremendous impact in recent decades [24]. The effectiveness of the CNNs is incontestable of which the non-local self-similarity techniques such as the TRND, BM3D purported for non-photographic image denoising performed abysmally lower compared to the CNNs which significantly its effectiveness with regard to less computational time among other qualities. Unlike, majority of denoising schemes pose complex and need vigorous effort and expensive optimization processes that lead to high computational cost, rather it is during the training stage that optimization is carried out using the CNN technique to effectively predict the denoised output from the noisy input. Notwithstanding, the inability of most recent architectures to explicitly determine the level of noise, are widely considered as the blind kind of denoising schemes [22]. Hence, in our work we successfully applied deep learning approach to intensively process a steady data stream over several hundreds of GB/s. As a result, the function is learned and then maps the input with the pairs of the output. The DnCNN is therefore carefully trained to predict the denoised 3D data from the 3D input data. Usually, a normal CNN architecture is comprised of an input layer, convolutional layers, and finally a regression or output layer. Hence these convolutional functions at this stage estimate the sliding dot outcome of the end product of the preceding layers with the desired filters. This is then followed by the application of a nonlinear activation notably the rectified linear unit (ReLU) to facilitate faster convergence of the network and to equally eliminate the gradient vanishing problems before the output progresses to the next batch of layer for processing. Therefore in the beginning of the training stage, the DnCNN network is given a 3D input data represented as *Y* of which the weights of the various learnable kernels are tuned during each epoch based training to reduce the deviation of the DnCNN output with respect to the ground truth data denoted as X. The purpose is to effectively retrieve a clean data $x \in X$ out of the noise data $y \in Y$. Hence, y is referred to as the superposition of the ground truth image data x with noise v expressed as $y = x + v$. General purpose signal denoisers must be tolerant enough to be able to be executed on any form of structural distributions in the data or image and should compromise for the processing of any high level frequency signals with outstretched uniform structures. Contrarily, the demonstration of the structural patterns in the image present particularized distribution, size, orientation and shape as illustrated in Fig 4 (a). It is lucid that the existence of these distinctive patterns emanated due to the interference of several Rayleigh scattering effect within the length of the pulse propagating on the sensing fiber. The prevalence of these features are mainly resulted as the functions of the bandwidth detection process, optical pulse duration, and the sampling rate. Intuitively, since the structural features exhibits relatively high level ratios, as well as prevailing orientation on the distance axis, the application of exact filters matching these kinds of ratios was executed to achieve the desire outcome. A critical assessment of the structural patterns and matching of the receptive field with the orientation and the structure stand to reduce the depth of the proposed technique and as a result, there is the need to equally enhance the DnCNN model with a good number of convolutional layers.

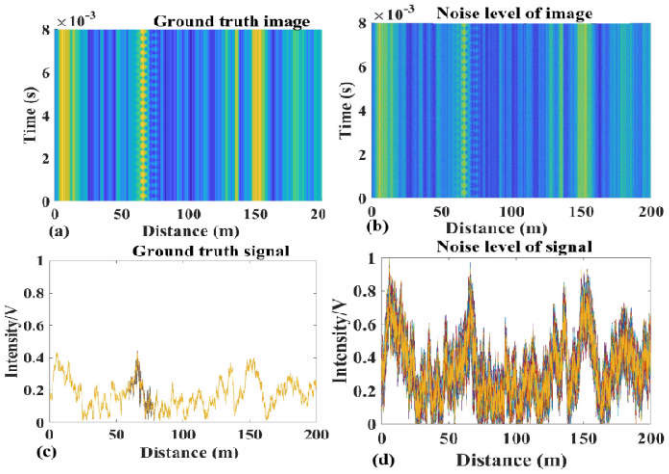

Fig 4 (a) Ground truth image (b) Noisy image (c) Ground truth signal (d) Noisy signal

In Fig. 4(b), the noise demonstrates some characteristic spatial patterns of the measured 3D noise concentration. Also, the intensity of the extreme noise level can be seen by comparing the ground truth signal (reference clean signal) in Fig. 4(c) and Fig. 4(d) which heavily demonstrates the jagged noise presence on the signal compared to its ground truth signal.

DnCNN Training Procedure for Denoising

To successfully demonstrate the performance of the DnCNN for training the Φ-OTDR sensing data, we first and foremost executed digital down conversion on the simulated Φ-OTDR data to obtain a zero-band signal. The training process was then incorporated with the BN function to speed up the process. The mini-batch adaptive moment estimation (adam) was used with a weight decay factor of 0.0001 of which the gradient decay factor equally was set to 0.95 and a value of mini-batch size used was 50. The dimension of the data is 4000×4000 whereby the patches size of $50 \times 50 \times 2$ was applied for the training. The model was trained based on 60 epochs and for each training epoch, the random patch pairs of the image and noise signal are combined as inputs of the DnCNN, and the corresponding noise signals are marked as the labels.

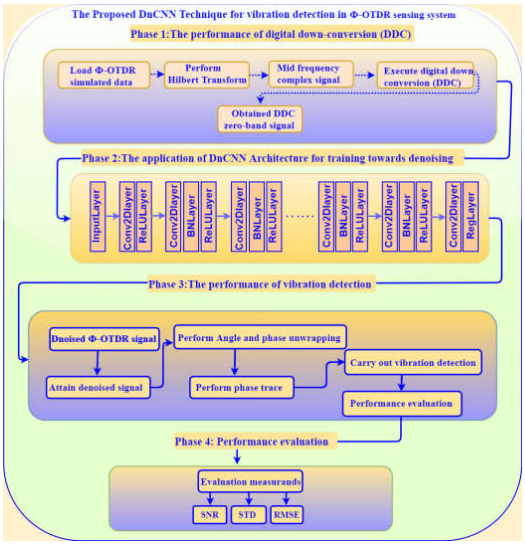

Fig 5 Flowchart of the proposed DnCNN based on Φ-OTDR vibration detection

A total of 195 iterations per one epoch was observed during the training of which an overall total of 11700 iterations were recorded during the entire training period. The learning rate is decayed exponentially with a value of 10^{-3} for the training of the 60 epochs. The training period took a total of 26 hours, 15 minutes to train the model based on Matlab (R2021a) program on a 64-bit window 10 operating system, thus an XPS Dell PC with a 16GB RAM powered by Core i7 CPU processor. To decrease the training time, the simplest way is to reduce the training data set, training epochs, or the network layers. However, in doing so the performance of the DnCNN may degrade and the target will not be achieved. The presentation of the DnCNN training for the purpose of attaining the vibration detection is illustrated in Fig. 5 above. The DnCNN predicts the noise data from the input data, then restores a clean data. During the training process, the parameters of the DnCNN are gradually optimized to minimize the difference between the acquired noise and the predicted result. Therefore, the trained DnCNN algorithm can be well adapted to the actual Φ-OTDR system towards the vibration detection. The strength of the DnCNN was tested against other state-of-the-art denoising techniques to comparatively determine its effectiveness as discussed in the subsequent sections.

The PCA denoising Stage of the Φ-OTDR data

In the principal component analysis setting, the Φ-OTDRnoisy signal is denoted as m × n dimensional aggregation, of which *m* signifies the number of transmission and *n* represents the stations unit. To acquire the sterling divergence, the data element coordinate system is turned til the first angle is on the tendency. Then the next number angle is selected for the subsequent number of variance dependent on the restraint that will be orthogonal to the initial order[29], thus

$$A=\begin{pmatrix} a_{11} & a_{12} & a_{13} & .. & a_{1n} \\ a_{21} & a_{22} & a_{23} & \dots & a_{2n} \\ \vdots & \vdots & \vdots & \vdots & \vdots \\ \vdots & \vdots & \vdots & \vdots & \vdots \\ a_{m1} & a_{m2} & a_{m3} & \dots & a_{mn} \end{pmatrix}, I=1,2,3,...,m; j=1,2,3,...,n \quad (5)$$

is the sample distribution matrix of a, where $a_1^j, j=1,2,3,...,n,$ are the discrete instances of $a_i, i=1,2,3,...,m.$ The i^{th} row of distribution matrix A is indicated by $A_i=[a_i^1, a_i^2, a_i^3 ..., a_i^n]$ and becomes the representative vector of a_i. The mean numerical quantity of A_i is computed as

$$\mu = \frac{1}{n}\sum_{j=1}^{n} A_i(j), \quad (6)$$

and the statistical distribution vector A_i is the centered matrix of A as declared in

$$\bar{A}_i = A_i - \mu_i = [\bar{a}_i^1, \bar{a}_i^2, \bar{a}_i^3, ..., \bar{a}_i^n], \quad (7)$$

where $\bar{a}_i^j = \bar{a}_i^j - \mu_i$. Consequently, the centered matrix of A is $\bar{A}_i = [\bar{a}_1^T, \bar{a}_2^T, \bar{a}_3^T ..., \bar{a}_m^T]^T$. Eventually, the covariance matrix of the centered input data is further measured as

$$\Lambda = \frac{1}{N}\overline{A}\,\overline{A}^T \quad (8)$$

where Λ is the covariance matrix of the centered input data $\overline{AA}^T$. The merit and focus of the PCA is, to effectively locate the orthonormiert transmutation matrix M to decorrelate A; thus, $D = MA$ such that the covariance matrix of D is diagonal. Once the covariance matrix Λ is symmetric, we define it as

$$\Lambda = \lambda \omega \lambda^T \quad (9)$$

of which $\lambda = [\lambda_1, \lambda_2, \lambda_3, ..., \lambda_m]$ becomes $m \times n$ orthonormal eigenvector matrix and $\omega = diag\{\omega_1, \omega_2, \omega_3, ..., \omega_m\}$ is the diagonal eigen value matrix with $\omega_1 \geq \omega_2 \geq \omega_3, ..., \geq \omega_m$. The $\lambda = \lambda_1, \lambda_2, \lambda_3, ..., \lambda_m$ and $\omega_1, \omega_2, \omega_3, ..., \omega_m$ hereby represent the eigenvectors and eigenvalues of λ. By transmutation $M = \phi^T$, $\bar{A}$ is decorrelated, to $\bar{D} = M\bar{A}$ and $\omega = \frac{1}{N}\overline{AA}^T$.

In conclusion, the energy of a signal will become concentrated on a minute set during the transformation of the dataset, whereas the energy level of the noise will be uniformly distributed over the entire dataset; thus, it totally decorrelates the simulatedΦ-OTDR noisy data thus $\overline{A}$, separating the signal from the noise for the enhancement of the desired denoised output.

RESULTS AND DISCUSSIONS

The Φ-OTDR simulation setup

Figure 6 illustrates the simulation setup based on the Φ-OTDR sensing technology for vibration detection of which an ultranarrow-line width laser of 100Hz operating at 1549.835nm is utilized as the source of light with the polarization-maintaining (PM) serving as the output. The laser output is then split into two channels by a 50:50 PM coupler. One of the channels is modulated by an in-phase/quadrature (I/Q) modulator operating at 50MHz frequency shift to generate the pulsed probe wave of 100ns pulse width with a sampling rate of 2GHz. The erbium-doped fiber amplifier (EDFA) is set into the optical path to increase the power of the pulse light for the enhancement of the intensity of the Rayleigh scattering (RS) light along the sensing fiber. The probe pulse is then injected into the sensing fiber through a circulator and the Rayleigh scattering signal is then injected into the 50:50 coupler. Another channel of the laser output is applied as the LO. Before the LO is injected into the 50:50 coupler, a polarization controller (PC) is inserted to match the LO with the selected polarization channel of the 50:50 coupler and before the 50:50 coupler there is the variable optical attenuator (VOA), which is used to adjust the powers of the LO. The two outputs of the 50:50 coupler are converted into the electrical E_Receive and E_Receive_noise (clean RS and noise RS signals) respectively by a two-port balanced photo-detector (BPD) and then sampled by the OSC at a position of 200m sensing fiber range. The external vibration source is simulated by a cylindrical piezo transducer (PZT) with a 12.7m bare fiber coiled around as the test point. Finally, the process leading to acquisition of data for training towards denoising, angle and phase unwrapping, and vibration detection are further completed in real time by the use of a personal computer.

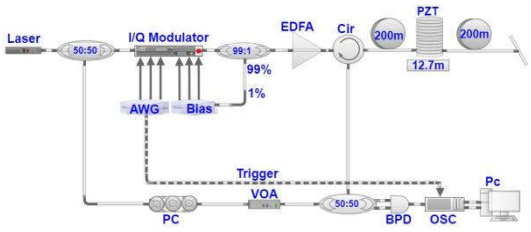

Fig 6 The Φ-OTDR simulation setup

Vibration extraction

After successfully denoising the DDC noisy data to obtain the desired denoised output for the purpose of unearthing the vibration point, the resulting complex time-domain signal was converted from the real and the imaginary format to the magnitude or phase format by the application of Eq. (10) as shown below. $\rho(t)=\sqrt{\ell^2(t)+h^2[\ell(t)]}$ (10)

We then performed angle and phase unwrapping algorithm to pave way for the vibration extraction using Eq. (11) and (12) expressed below;

$$\varphi(t)=unwrap[\angle(\varepsilon)] \tag{11}$$

of which ε represents the zero-band complex signal after denoising, and $\angle(\varepsilon)$ signifies taking the angle of the DDC noisy signal and after which, $\varphi(t)$ is successfully retrieved to aid the process of phase trace.

After locating the external perturbation, the phase information of the vibration signal is further accomplished by the phase difference execution. The phase change within the gauge length Δz can be expressed as shown in Eq. (12).

$$\Delta\varphi=\varphi(z)-\varphi(z-\Delta z) \tag{12}$$

which is linearly associated with the strain induced by the external vibration. Since there is a phase accumulation process when the pulse light passes through the perturbation zone, the gauge length must be greater than the sum of the vibration area (~2m) as well as the region influenced by the vibration. As the space occupied by the probe pulse is 20m, the region influenced by the vibration covers from 21m to vibration point and 19m after the perturbation area. As stated in the receding, the gauge length is twice the theoretical resolution which leads to better SNR achievement. As a result, the measurand with respect to the SNR and Root Mean Square Error were then computed and analyzed. Therefore, the corresponding statistical features and desired information was extracted to reveal the vibration points on the time domain signals. The SNR and Root Mean Square Error are then computed of which the SNR is expressed as the ratio of the power of the clean signal (meaningful information) to the power of background noisy signal (unwanted signal). The signal power and the noise power are hereby represented as;

$$P_S=var(y) \tag{13}$$

where y is the desired signal without noise (fitted curve) and $var(\cdot)$ is the variance. On the other hand, the noise power of the signal is also represented as

$$P_N=var(s-y) \tag{14}$$

of which s is the simulated signal with noise. As stated above, the SNR is expressed as shown in

$$SNR=10\log 10\left(\frac{P_S}{P_N}\right) \tag{15}$$

where P_S and P_N indicate the signal power and noise power.

Analysis of DnCNN and PCA Results

As previously stated, digital down-conversion was performed on the simulated Φ-OTDR data which was initially a mid-band signal to obtain a zero-band signal (complex signal) where Eq. (1), (2), and Eq. (3) were respectively employed to harness an effective application of the proposed DnCNN and the PCA denoising technique. The desired denoised signals were then successfully achieved. Hence, the results of the original signal and its corresponding denoised signals are demonstrated in Figs. 7(a), (b) and (c) representing the original signal, DnCNN denoised signal and PCA denoised signal respectively below. It is evident that there is a significant diminution of the noise level per the denoised results by the proposed technique compared to the denoised results of the PCA with respect to the presence of extreme noise observed on the original signal, as shown in Fig. 7 below.

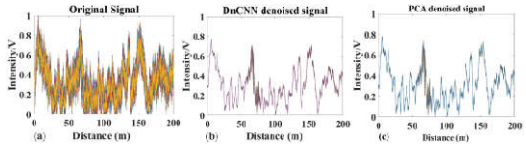

Fig 7 (a) Original signal (b) DnCNN denoised (c) PCA denoised

In order to achieve the target of this research, the desired denoised results by the proposed and the other state-of-the-art denoising approach were respectively obtained and the performance of angle and phase unwrapping, differential phase trace were duly executed to enhance the vibration detection along the fiber under test by the application of Eq. (10), (11) and (12), respectively.

Vibration Extraction

The output of the normalized demodulated reflection of the intensity traces are respectively constructed and compared with the denoised normalized intensity trace signals, as illustrated in Fig 8. Constructively, the performance enhancement can be observed per the reflection of the intensity trace on the original signals appearing to be extremely notched due to the presence of much interference and fading effect, thereby leading to the demonstration of exceedingly weak fading points as comparatively presented below whereby all categories of (a) represent the original data, (b) DnCNN denoised results, (c) PCA denoised results of which the proposed technique yielded the best result,

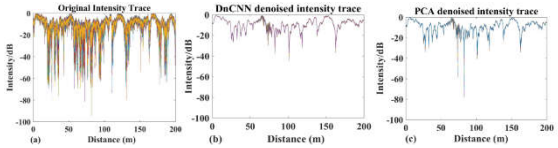

Fig 8 (a) Original intensity trace (b) DnCNN denoised (c) PCA denoised

In the field of signal processing, telecommunications, optical imaging, among others, fading has been an obstacle. The said phenomenon posses devastating influence on signals, which sometimes becomes very arduous to precisely locate the vibrations after denoising, all due to the presence of the phase extraction noise in the differential phase traces.

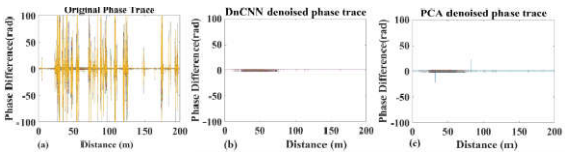

Fig. 9 (a) Original phase trace (b) DnCNN denoised (c) PCA denoised

Nevertheless, the proposed DnCNN successfully handled the said plight significantly towards the target denoised signal, which facilitated the extraction of the normalized denoised phase traces as presented in Fig. 8. Therefore a comparative analysis with respect to the performances of the proposed and the PCA denoising techniques are objectively demonstrated of which the proposed technique outperformed it. However, to further confirm the performance strengths of the aforementioned denoising techniques, the computation of the signal-to-noise-ratio (SNR), the standard deviation (STD) as well as the affirmation of the SNR enhancement were respectively performed during the extraction of the time domain signals. Comparatively a presentation of the time domain signals regarding the original time domain, DnCNN denoised time domain and the PCA denoised time domain are hereby illustrated in Fig. 10.

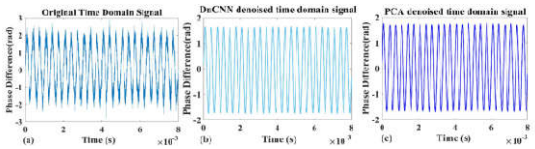

Fig. 10 (a) Original Time domain signal (b) DnCNN denoised time domain signal (c) PCA denoised time domain signal

There was an overwhelming improvement of the SNR value from 15dB to 36.6dB corresponding to both the original and denoised time domain signals, respectively by the proposed DnCNN technique whereas the PCA obtained an SNR value of 33.5dB, by the application of Eq. (15).

In addition, to reassert the SNR enhancement, the computation of standard deviation (σ^2) per the various detected vibration points on the dataset by the application of Eq. (16) as expressed below;

$$\sigma^2 = \sqrt{var(x-y)} \tag{16}$$

where x represents the signal with noise, and y indicates the desired signal without noise. We therein obtained 0.3198 and 0.0116, as the values corresponding to the standard deviation of the original noisy signal and denoised signal respectively by the DnCNN denoising technique. Hence, the determination of the SNR enhancement level was finally calculated by the application of Eq. (17).

$$\Delta SNR = 10\log 10\left(\frac{\sigma^2 x}{\sigma^2 y}\right) \tag{17}$$

As a result, an approximation value of 21.6dB was obtained as the SNR enhancement by the proposed method whereas the PCA technique that obtained its y value of 0.0180 and x value is 0.3198 which represents the noisy signal, equally achieved an SNR enhancement value of approximately 18.5dB.The illustration of the measured simulated and fitted curve performance with respect to the proposed DnCNN and PCA are respectively shown in Fig.11 below. The performance of the proposed technique by visual impression lucidly outperformed that of the contested PCA.

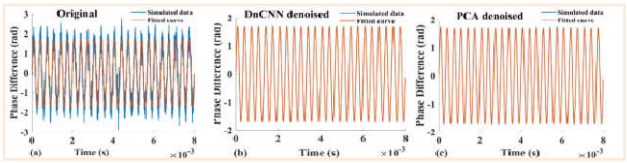

Fig 11(a) Original and fitted curve (b) DnCNN denoised data with fitted curve (c) PCA denoised data with fitted curve

The root-mean-square-error (RMSE) values were equally executed to measure the performance of each of the contested methods by the application of Eq. (18) as presented below.

$$RMSE = \sqrt{\frac{1}{n}\sum_{i=1}^{n}\left(\hat{y}_i - y_i\right)^2} \tag{18}$$

where the noisy data is represented as $\hat{y}_i$ and y_i indicates the predicted or denoised signal. The DnCNNand PCA both derived values of 0.12, and 0.20 respectively.

CONCLUSION

In this paper, a DnCNN based on Φ-OTDR sensing data for vibration detection is demonstrated. The Φ-OTDR noisy data was acquired to train the DnCNN model of which it yielded the desired denoised outputs towards precised detection of the

vibration point along the sensing fiber. The proposed technique equally demonstrated significant performance with respect to the SNR enhancement, as well as a good range of RMSE and STD values. In order to justify the efficiency and efficacy of the proposed technique, it was tested against one key state-of-the-art (PCA) denoising technique which equally preserved good structural information for the vibration extraction. Emphatically stating, the proposed technique proved robust enough per the total annihilation of all the fading points compared to the principal component analysis approach. Per these meritorious and effectiveness of the proposed method, once a sensing system is settled on, the DnCNN is capable of effectively learning to adapt in order to produce the desired results. In conclusion, the application of deep learning is evolving very rapidly and the DnCNN denoising technique has practically demonstrated its capabilities in facilitating effective DOVS applications and could be replicated in other related fields of study.

Acknowledgement: This work is partly supported by the Zhoukou Normal University super scientific project ZKNUC2018019.

Disclosures. Thispaper presents an original work and we hereby declare no conflict of interest relative to other works.

References

1. L. Thevenaz "Next generation of optical fifibre sensors: new concepts and perspectives", Proc. SPIE 9157, 23rd International Conference on Optical Fibre Sensors, 9157AN (2014).
2. L. Zhang, Z. N. Wang, J. Li, J. J. Zeng, X. H. Jia, and Y. J. Rao, "Ultra-long dual-sideband BOTDA with balanced detection," Opt. Laser Technol. 68, 206-210 (2015).
3. Z. N. Wang, J. J. Zeng, J. Li, M. Q. Fan, H. Wu, F. Peng, L. Zhang, Y. Zhou, and Y. J. Rao, "Ultra-long phase sensitive OTDR with hybrid distributed amplifification," Opt. Lett. 39(20), 5866-5869 (2014)
4. S. Martin-Lopez, M. Alcon-Camas, F. Rodriguez, P. Corredera, J. D. Ania-Casta Ã´ son, L. Thevenaz, and M. Gonzalez-Herraez, "Brillouin optical time-domain analysis assisted by second-order Raman amplifification," Opt. Express 18(18), 18769-18778 (2010).
5. H. Martins, S. Martin-Lopez, P. Corredera, J. D. AniaCastanon, O. Frazao, and M. Gonzalez-Herraez, "Distributed vibration sensing over 125km with enhanced SNR using phi-OTDR over an URFL cavity," J. Lightwave Technol. 33(12), 2628-2632 (2015).
6. D. Chen, Qingwen Liu, and Zuyuan He. "Phase-detection distributed fiber-optic vibration sensor without fading noise-noise based on time-gate digital OFDR", Vol.25, No. 7| 3 Apr 2017 | OPTICS EXPRESS 8315
7. B. Ha Lee, Young Ho Kim, Kwan Seob Park, Joo Beom Eom, Myoung Jin Kim, Byung Sup Rho, and Hae Young Choi," Interferometric Fiber Optic Sensors" Sensors , 12, pp.2467-2486,2012.
8. H. Wu, C. Zhao, R. Liao, Y. Chang, and M. Tang, "Performance enhancement of ROTDR using deep convolutional neural networks," in 26th International Conference on Optical Fiber Sensors (2018) (Optical Society of America, 2018), paper TuE16. 29
9. Y. Shi, Y. Wang, L. Zhao, and Z. Fan, "An event recognition method for Φ-OTDR sensing system based on deep learning," Sensors 19(15), 3421 (2019). 30
10. L. Shiloh, A. Eyal, and R. Giryes, "Efficient Processing of Distributed Acoustic Sensing Data Using a Deep Learning Approach," J. Lightwave Technol. (2019), 37(18), 4755–4762
11. M. Aktas, T. Akgun, M. U. Demircin, and D. Buyukaydin, "Deep learning based multi-threat classification for phase-OTDR fiber optic distributed acoustic sensing applications," Proc. SPIE (2017), 10208, 102080G .
12. J. Tejedor, J. Macias-Guarasa, H. F. Martins, J. Pastor-Graells, P. Corredera, and S. Martin-Lopez, "Machine learning methods for pipeline surveillance systems based on distributed acoustic sensing: A review," Appl. Sci. (2017), 7(8), 841.
13. Q. Sun, Q. Li, L. Chen, J. Quan, and L. Li, "Pattern recognition based on pulse scanning imaging and convolutional neural network for vibrational events in Φ-OTDR," Optik (2020), 219, 165205.
14. Z. Wang, S. Lou, X. Wang, S. Liang, and X. Sheng, "Multi-branch long short-time memory convolution neural network for event identification in fiber-optic distributed disturbance sensor based on φ-OTDR," Infrared Phys. Technol.(2020), 109, 103414.
15. Y. Shi, Y. Wang, L. Wang, L. Zhao, and Z. Fan, "Multi-event classification for Φ-OTDR distributed optical fiber sensing system using deep learning and support vector machine," Optik (2020), 221, 165373 .
16. Y. Bai, J. Xing, F. Xie, S. Liu, and J. Li, "Detection and identification of external intrusion signals from 33 km optical fiber sensing system based on deep learning," Opt. Fiber Technol. (2019), 53, 102060.
17. S. Liehr, L. A. Jäger, C. Karapanagiotis, S. Münzenberger, and S. Kowarik, "Real-time dynamic strain sensing in optical fibers using artificial neural networks," Opt. Express (2019), 27(5), 7405–7425.
18. A. Simonyan, Zisserman, "Very deep convolutional networks for large-scale image recognition," in International Conference for Learning Representations, (2015)
19. A. Krizhevsky, I. Sutskever, and G. E. Hinton, "Imagenet classification with deep convolutional neural networks," in Advances in Neural Information Processing Systems, (2012), pp. 1097–1105.
20. S. Ioffe and C. Szegedy, "Batch normalization: Accelerating deep network training by reducing internal covariate shift," in International Conference on Machine Learning, (2015), pp. 448–456.
21. K. He, X. Zhang, S. Ren, and J. Sun, "Deep residual learning for image recognition," in IEEE Conference on Computer Vision and Pattern Recognition, (2016), pp. 770–778.
22. K. Zhang, W. Zuo, Y. Chen, D. Meng, and L. Zhang, "Beyond a Gaussian denoiser: Residual learning of deep CNN for image denoising," IEEE Trans. Image Process., (2017), vol. 26, no. 7, pp. 3142–3155.
23. K. Simonyan and A. Zisserman, "Very deep convolutional networks for large-scale image recognition," in International Conference for Learning Representations, (2015).
24. H. Wu,, Yangyang Wan, Ming Tang, Real-Time Denoising of Brillouin Optical Time Domain Analyzer With High Data Fidelity Using Convolutional Neural Networks, Journal of Lightwave Technology, (2019). Vol. 37, No. 11.
25. B. Dong, V. Tribaldos, X. Xing, S. Byna, J. Ajo-Franklin, and K. Wu, "DASSA: Parallel DAS Data Storage and Analysis for Subsurface Event Detection," IEEE International Parallel and Distributed Processing Symposium (IPDPS) (2020).
26. H. F. Taylor and C. E. Lee, "Apparatus and method for fiber optic intrusion sensing," U.S. patent 5,194,847 (March 16, 1993).
27. A. H. Hartog, An Introduction to Distributed Optical Fibre Sensors, 1st ed. (CRC Press, (2017).
28. Z. N. Wang, J. Li, M. Q. Fan, L. Zhang, F. Peng, H. Wu, *et al*., "Phase-sensitive optical time-domain reflectometry with Brillouin amplification," Optics Letters, (2014), 39(15): 4313–4316.
29. A. Farag and S. Elhabian, A Tutorial on Principal Component Analysis (University of Louisville, CVIP lab, 2009).

****